

UCLA

UCLA Previously Published Works

Title

Vestibular Drop Attacks and Meniere's Disease as Results of Otolithic Membrane Damage—A Numerical Model

Permalink

<https://escholarship.org/uc/item/3v5343b6>

Journal

Journal of the Association for Research in Otolaryngology, 24(1)

ISSN

1525-3961

Authors

Senofsky, Nicholas

Faber, Justin

Bozovic, Dolores

Publication Date

2023-02-01

DOI

10.1007/s10162-022-00880-0

Copyright Information

This work is made available under the terms of a Creative Commons Attribution License, available at <https://creativecommons.org/licenses/by/4.0/>

Peer reviewed



Vestibular Drop Attacks and Meniere's Disease as Results of Otolithic Membrane Damage—A Numerical Model

Nicholas Senofsky¹ · Justin Faber¹ · Dolores Bozovic^{1,2}

Received: 20 February 2022 / Accepted: 20 November 2022 / Published online: 14 December 2022
© The Author(s) 2022

Abstract

Meniere's disease (MD) is a condition of the inner ear with symptoms affecting both vestibular and hearing functions. Some patients with MD experience vestibular drop attacks (VDAs), which are violent falls caused by spurious vestibular signals from the utricle and/or saccule. Recent surgical work has shown that patients who experience VDAs also show disrupted utricular otolith membranes. The objective of this study is to determine if otolith membrane damage alone is sufficient to induce spurious vestibular signals, thus potentially eliciting VDAs and the vestibular dysfunction seen in patients with MD. We use a previously developed numerical model to describe the nonlinear dynamics of an array of active, elastically coupled hair cells. We then reduce the coupling strength of a selected region of the membrane to model the effects of tissue damage. As we reduce the coupling strength, we observe large and abrupt spikes in hair bundle position. As bundle displacements from the equilibrium position have been shown to lead to depolarization of the hair-cell soma and hence trigger neural activity, this spontaneous activity could elicit false detection of a vestibular signal. The results of this numerical model suggest that otolith membrane damage alone may be sufficient to induce VDAs and the vestibular dysfunction seen in patients with MD. Future experimental work is needed to confirm these results *in vitro*.

Keywords Meniere's disease · Vestibular drop attacks · Amplitude death · Nonlinear dynamics · Vestibular function

Introduction

Meniere's disease (MD) is a condition of the inner ear affecting both vestibular and hearing functions. MD occurs in 17 people out of 100,000, and adequate treatment options are scarce. In some cases, clinicians resort to gentamicin profusions, vestibular neurectomies, or even labyrinthectomies to reduce or eliminate vestibular activity [1]. MD can cause episodic vertigo, hearing loss, tinnitus, and excessive pressure in the inner ear, with symptoms occurring either unilaterally or bilaterally [1]. In rare cases, patients affected by MD can suffer from vestibular drop attacks (VDAs), which are characterized by a sudden, forceful loss of balance. The cause of vestibular drop attacks is currently

unknown. However, recent work by Calzada has suggested that the presence of VDAs among patients with MD can be attributed to damage of the otolith membrane tissue in the utricle and/or saccule [2]. Calzada found that all patients who experience VDAs show disrupted utricular otolith membranes. Additionally, Calzada showed that the average thickness of the utricular otolith membrane in patients with MD is 11.45 μm , while in normal tissue, the mean thickness is 38 μm . Patients often report multiple vestibular drop attacks, with the resulting falls occurring in the same direction each time, suggesting a spurious vestibular signal. Meniere's disease is highly correlated with endolymphatic hydrops. However, the two conditions are clinically distinct from each other, and the mechanisms causing MD are currently unknown [3].

The utricle and saccule rely on hair cells to detect linear accelerations. These specialized sensory cells are named after the rodlike stereovilli that protrude from their apical surface. The stereovilli are collectively named the hair bundle, which pivots in response to acceleration. This deflection of the hair bundle modulates the tension in the tip links that connect adjacent rows of stereovilli and controls the gating

✉ Nicholas Senofsky
nicholassenofsky@gmail.com

¹ Department of Physics and Astronomy, Physics and Astronomy Building, University of California, 430 Portola Pl, Los Angeles, CA, USA

² California NanoSystems Institute, University of California, Los Angeles, CA 90095, USA

of mechanotransduction channels embedded in the tips of the stereovilli. Therefore, hair cells transduce the mechanical energy of acceleration into electrical energy in the form of ionic currents into the cell [4–6]. The response of the inner-ear hair cells to incoming signals has been shown to be highly nonlinear, in a compressive manner, allowing them to exhibit a broad dynamic range [7]. Furthermore, hair cells produce active amplification, enhancing weak signals and thus endowing auditory and vestibular systems with high sensitivity [8].

Hair-cell bundles of certain species have been shown to exhibit innate motility in the absence of stimulus [9, 10]. In the amphibian sacculus, these spontaneous oscillations have amplitudes significantly larger than the motion induced by thermal fluctuations in the surrounding fluid. These innate oscillations have been shown to be active, powered by an energy-consuming process [11]. While they have been proposed to assist in the amplification of weak signals, or possibly underlie the generation of otoacoustic emissions by the inner ear, the presence or role of these spontaneous oscillations in vivo is currently unknown. Experiments performed in vitro on the amphibian sacculus, however, have shown that these active oscillations are suppressed by the presence of the overlying otolithic membrane [12]. In healthy tissue, the otolithic membrane connects to the tops of the hair bundles and provides mechanical coupling between them [13, 14]. This inter-cell coupling is sufficiently strong to suppress the innate motility of individual bundles, poisoning the full coupled system in the quiescent regime. Only after digestion and careful removal of this membrane have spontaneous hair bundle oscillations been observed. In this study, we explore the possibility that MD results from degraded or missing otolithic membrane tissue in the utricle or saccule. Specifically, we hypothesize that locally degraded coupling between hair cells can lead to the sudden onset of spontaneous oscillations in a subset of bundles, leading to a spurious signal that may cause VDAs and the vestibular dysfunction seen in patients with MD.

We use a previously developed numerical model to describe the nonlinear dynamics of an array of active hair cells. We introduce elastic coupling between nearest and next-nearest neighbors on the grid, representing the mechanical connection between cells imposed by the otolithic membrane tissue. We introduce heterogeneity in the selection of the model parameters to produce spatially random dispersion in the characteristic frequencies of the hair cells, approximating that of the saccule. This frequency dispersion suppresses the autonomous motion of the hair bundles, resulting in a quiescent system. We then reduce the coupling strength of a selected region of the membrane to model the effects of tissue damage. In order to compare the results of our simulations to empirical data, we base our parameter selections

on those obtained from the bullfrog sacculus. This is due to the sacculus having yielded the most extensive experimental measurements that are applicable to our model. Our choice of model species does not limit the results of our model as we are exploring the general phenomenon of how localized changes in coupling affect the dynamics of the system. The dynamics of coupled nonlinear oscillators examined in our model is applicable to the mammalian vestibular system as we have avoided any extraneous terms which are not necessary to reproduce the dynamics of hair cells coupled by the otolithic membrane. We explore the dynamics for several levels of tissue damage and find that large, abrupt spikes in hair bundle position emerge, with larger and more frequent spikes occurring for increasing levels of tissue damage. These spikes in bundle position correspond to large spikes in the opening probability of the transduction channels, which would hence elicit significant neural activity [15]. We, therefore, propose that aspects of the vestibular dysfunction attributed to Meniere's disease arise from degradation in the otolithic membrane tissue, which reduces the coupling strength imposed by the membrane, resulting in large, abrupt spikes in the positions of the hair bundles.

Methods

To explore the impact of Meniere's disease in a numerical simulation, we model the sacculus as a system of coupled nonlinear oscillators. The mechanical motility of individual hair bundles is described using previously established biophysical models, which have been shown to reproduce a broad set of experimental results [16, 17]. We model the coupled system as a 15 by 15 grid of hair cells, with each cell connected to its nearest and next-nearest neighbors (Fig. 1). To simulate localized damage to the otolithic membrane, we impose varying levels of reduction in the coupling coefficient, K_d , within the damaged region (shown in blue in Fig. 1). Empirical measurements of the extent by which coupling is reduced upon OM damage are not known. We thus vary the reduction in coupling such that it does not exceed an order of magnitude, an estimate likely to be conservative given the surgical findings [2]. Furthermore, coupling coefficients in healthy tissue have been based on work by Ji et al. [18]. Outside of the damaged region, the coupling constants, K , are held constant to represent healthy otolithic membrane tissue. The coupling mediated by viscous forces is very weak when compared to the elastic coupling and is thus neglected in this study [13, 14].

The equations of motion for the bundles of each individual hair cell are as follows:

$$\frac{\lambda}{a_0[i,j]} \frac{dX}{dt} = -K_{gs}(X - X_a - DP_o) - K_{sp}X + F_K + \eta \quad (1)$$

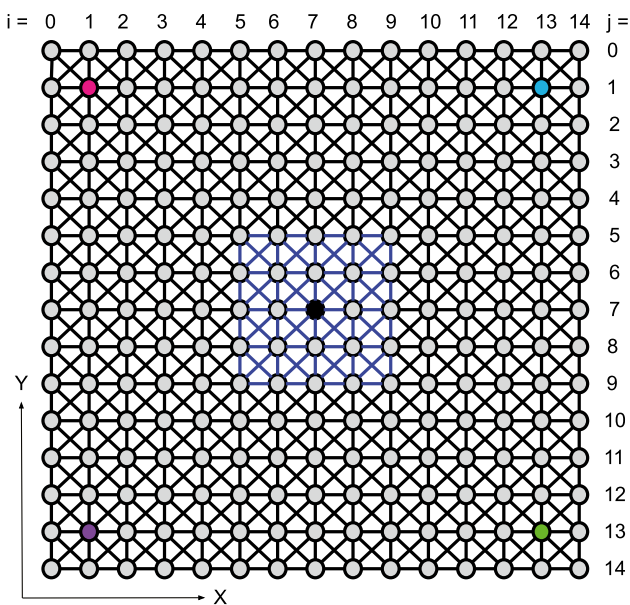


Fig. 1 Grid of 15×15 coupled hair bundles, each represented by a circle. The black lines represent springs with coupling constant, K , and blue lines represent springs with coupling constant K_d , which are varied to simulate damage to the membrane. Colored circles represent the bundles used to compare the dynamics of bundles under normal coupling conditions to those with a damaged membrane. The black circle represents the bundle in the damaged region that will be examined

$$\frac{\lambda_a}{a_0[i,j]} \frac{dX_a}{dt} = K_{gs}(X - X_a - DP_o) - \gamma N_a f[i,j] p(C) + K_{es}(X_a + X_{es}) + \eta_a \tag{2}$$

$$\frac{\tau}{a_0[i,j]} \frac{dC}{dt} = C_0 - C + C_M P_o + \delta c \tag{3}$$

X represents the position of the hair bundle, X_a represents the position of the myosin motor, and C represents the Ca^{2+} concentration at the myosin motor binding site. λ and λ_a represent damping coefficients for the hair bundle and myosin motor, respectively. The hair bundle is subject to forces from the gating spring and the stereociliary pivots, which have characteristic stiffnesses K_{gs} and K_{sp} , respectively. D represents the elongation of the gating spring caused by the transduction channel opening. At stall, the motors produce an average force of $\gamma N_a f p$, where f is the force of an individual motor, p is the probability that a motor is bound to an actin filament, N_a represents the number of motors within a hair bundle, and γ is a dimensionless parameter that represents the geometrical gain from stereociliary shear. τ represents the time constant of calcium feedback, while C_0 and C_M represent the minimum and maximum calcium concentrations at the motor, respectively.

Experimental studies of hair bundle motion have established that there is only one axis along which deflection

results in changes in the channel opening probability. Furthermore, the active process operant in hair-bundle motion likewise acts along the same axis of sensitivity [10]. Hence, hair bundles in the model are restricted to one-dimensional motion along the x -axis, as defined in Fig. 1. Furthermore, apart from the striola, hair bundles in a given area of the sacculus point in approximately similar directions. The small variation in the angles would merely result in different projections along the mean axis of oscillation and hence is accounted for by variation in the amplitude of oscillation.

Each hair bundle’s transduction channel is viewed as having two states, open or closed, with open probability,

$$P_o = \frac{1}{1 + A e^{-\frac{X - X_a}{\delta}}} \tag{4}$$

where $A = \exp([\Delta G + (K_{gs} D^2)/(2N)]/(k_b T))$, and $\delta = N k_b T / (K_{gs} D)$. ΔG represents the intrinsic energy change upon channel opening, and k_b is the Boltzmann constant.

The force generated by a single myosin motor is given by $f[i,j] = f_{max}[i,j]/(N_a P_o)$, where each element of $f_{max}[i,j]$ is randomly sampled from a uniform distribution ranging from 87 to 352 pN. The unitless feedback parameter, S , and the maximal force f_{max} define the dynamic state of the hair bundle, poising it in the oscillatory, bistable, or quiescent regime, or near a bifurcation between the different regions. Using this model, prior studies have established a full state diagram and defined the boundaries delineating these regions. Two specific points were identified within the diagram: the point at which a bundle would exhibit the greatest sensitivity, as well as a point that best describes the experimentally determined state; both points reside within the oscillatory region of the state diagram [17].

We modify the model of Nadrowski et al. to include an additional term in the equation of motion for the myosin motors. The term was introduced in prior literature to describe the experimental observation that myosin-mediated adaptation is not complete [10, 19]. This effect is represented by an additional elastic spring, which opposes adaptation. K_{es} represents the coefficient of this extent spring, and X_{es} describes the position of the spring relative to the myosin motors [20]. The extent spring has been included, as it was shown crucial in describing the effects of mechanical offset on the dynamics of the bundle. In a prior study, we showed that mechanical offset strongly impacts the hair cell motility [12]. In numerical models, this could only be reproduced with the inclusion of the extent spring [20].

To mimic the natural variation of hair bundle states in a sacculus, we vary the parameters in the numerical model of each oscillator, thus leading to a dispersion in their innate frequencies (Fig. 2). Furthermore, the selection of parameters leads to a variation in the dynamic state exhibited by each bundle. As an approximation of this dispersion, we assume that they are all poised in the oscillatory state and

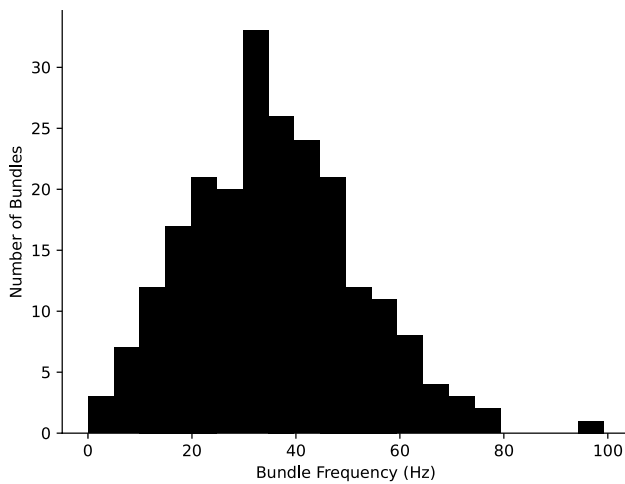


Fig. 2 Frequency distribution of 15×15 uncoupled hair bundles. The a_0 , S and f_{max} values were randomly selected for each hair bundle

sample the position of each bundle uniformly along the line segment described as follows. The probability that myosin motors are bound to actin is given by $p(C) = p_0 + p_1[i, j]C$. p_0 is fixed to 0.2, and each p_1 value is sampled in such a manner that the dimensionless feedback parameter S is linearly related to f_{max} ($S = -C_M p_1 / p_0$); this choice allows us to sample a region of the state space in which oscillatory hair bundles have been shown to reside. This sampling of

the phase space and the inclusion of frequency dispersion renders any changes in the state diagram due to the introduction of the extent spring negligible for modeling experimental measurements of hair bundle motion. We have obtained similar results when poisoning all of the oscillators in regions of the oscillatory region closer to the Hopf bifurcation.

Prior experimental studies have shown that hair cells of an amphibian sacculus show a random distribution of innate oscillation frequencies. We assume a comparable distribution in our model and assign each hair cell a characteristic a_0 , randomly selected from a normal distribution of mean 1.5 and standard deviation 0.25. These a_0 values ensure that the frequency distribution of uncoupled hair bundles in our model matches the measured frequency distribution of spontaneous oscillations in the bullfrog sacculus [21]. The frequency dispersion applied in this numerical model is shown in Fig. 2. This dispersion has been selected to match the frequency distribution of spontaneously oscillating hair cells in the bullfrog sacculus, as measured with high-speed video [21]. Each hair bundle thus has its own individual values of a_0 , S , and f_{max} that remain fixed for the duration of each trial. The bundles' frequencies and their locations in the state space are varied independently of each other to reflect the different sources of variation observed in experimental measurements.

Each equation is subject to white Gaussian noise, with zero mean and correlation functions as follows:

Table 1 Parameters of the numerical model. K and d are taken from [16]. Values for K_{es} and X_{es} are taken from [20], and all other parameters are taken from [17]

Constant	Value	Description
λ	$2.8 * 10^{-6}$ Ns/m	Friction coefficient of hair bundle
λ_a	$10 * 10^{-6}$ Ns/m	Friction coefficient of adaptation motors
K_{gs}	$750 * 10^{-6}$ N/m	Combined gating spring stiffness
K_{sp}	$600 * 10^{-6}$ N/m	Combined stiffness of stereociliary pivots and load
K_{es}	$140 * 10^{-6}$ N/m	Stiffness of extent spring
X_{es}	$20 * 10^{-9}$ m	Resting deflection of extent spring
d_{gs}	$8.7 * 10^{-9}$ m	Gating-spring elongation on channel opening
γ	0.14	Geometrical gain of stereociliary shear motion
τ	$0.1 * 10^{-3}$ s	Time constant of calcium feedback
τ_c	$1 * 10^{-3}$ s	Dwell time of transduction channels
C_0	0 M	Intracellular Ca^{2+} concentration with closed channels (theoretical approximation to 100 nM, the lowest observed intracellular concentrations)
N	50	Number of stereocillia
N_a	3000	Number of motors in the hair bundle
k_b	$1.38 * 10^{-23}$ J/K	Boltzmann constant
T	300 K	Temperature
ΔG	$4.14 * 10^{-20}$ J	Gibbs free energy for MET channel opening
T_a	1.5 * T	Effective temperature for noise strength of motor position
D	d_{gs}/γ	Displacement due to gating spring
C_{Max}	$250 * 10^{-3}$ M	Maximum calcium concentration at motor
d	$50 * 10^{-6}$ m	Distance between hair bundles
K	0.0014 N/m	Combined stiffness of the membrane, hair bundles, and filaments

$$\langle \eta(t)\eta(t') \rangle = 2k_b T \lambda \delta(t - t') \tag{5}$$

$$\langle \eta_a(t)\eta_a(t') \rangle = 2k_b T_a \lambda_a \delta(t - t') \tag{6}$$

$$\langle \delta c(t)\delta c(t') \rangle = 2C_M^2 N^{-1} P_o(1 - P_o)\tau_C \delta(t - t') \tag{7}$$

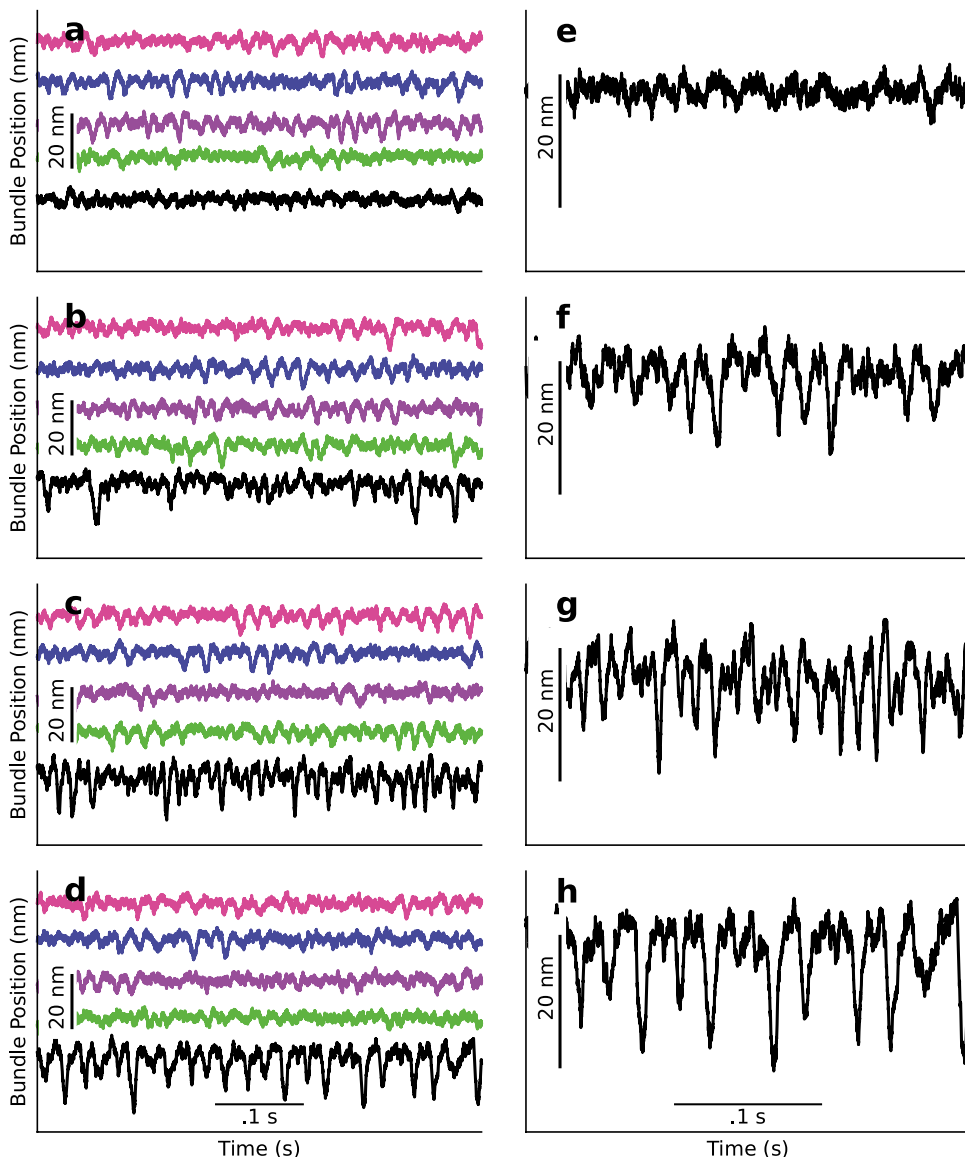
where the angle brackets denote the time average and δ represents the Dirac delta function. T and T_a represent the temperature of the system and the effective temperature of the motors. τ_C represents the dwell time of the transduction channels. The force exerted on each bundle due to coupling to nearest and next-nearest neighbors is given by

$$F_k(K_v) = K_v \left(1 - \frac{L_0}{\sqrt{(\Delta X + kd)^2 + (ld)^2}} \right) (\Delta X + kd) \tag{8}$$

where ΔX is the difference in the positions of the two bundles connected by the coupling spring, and $L_0 = \sqrt{(k^2 + l^2)d^2}$. d is the distance between nearest neighbors, while k and l are integers that represent the relative position between bundles on the grid. k is the row of the first bundle minus the row of the second, and l is the column of the first bundle minus the column of the second. This notation accounts for the fact that nearest neighbors are closer together than next-nearest neighbors [16].

$K_v = K$ in healthy tissue, and $K_v = K_d$ in damaged tissue, as shown in Fig. 1. We vary K_d in order to explore the dynamics of the coupled system for different degrees of damage to the otolithic membrane tissue. The coupled differential equations were solved numerically using a fourth-order Runge–Kutta method with time steps of 20 μ s. We note that the original model contains offsets in X , X_a , and C ;

Fig. 3 a–d Traces of bundle position with $K_d = K, K/5, K/10,$ and $K/15$, respectively. The colors of each trace represent the colored bundles in Fig. 1. The black bundle resides in damaged tissue, while the rest reside in healthy tissue. Arbitrary offsets have been added to the traces for clarity. **e–h** Zoomed in plots of the black traces in **a–d**



as these offsets reflect an arbitrary choice of a zero point and do not affect the bundle dynamics, we have elected to retain them in our adaptation of this model [16]. Parameter values were adopted from Nadrowski et al. and Julicher et al. and can be found in Table 1 [16, 17]. Source code for running these simulations can be found on GitHub [22].

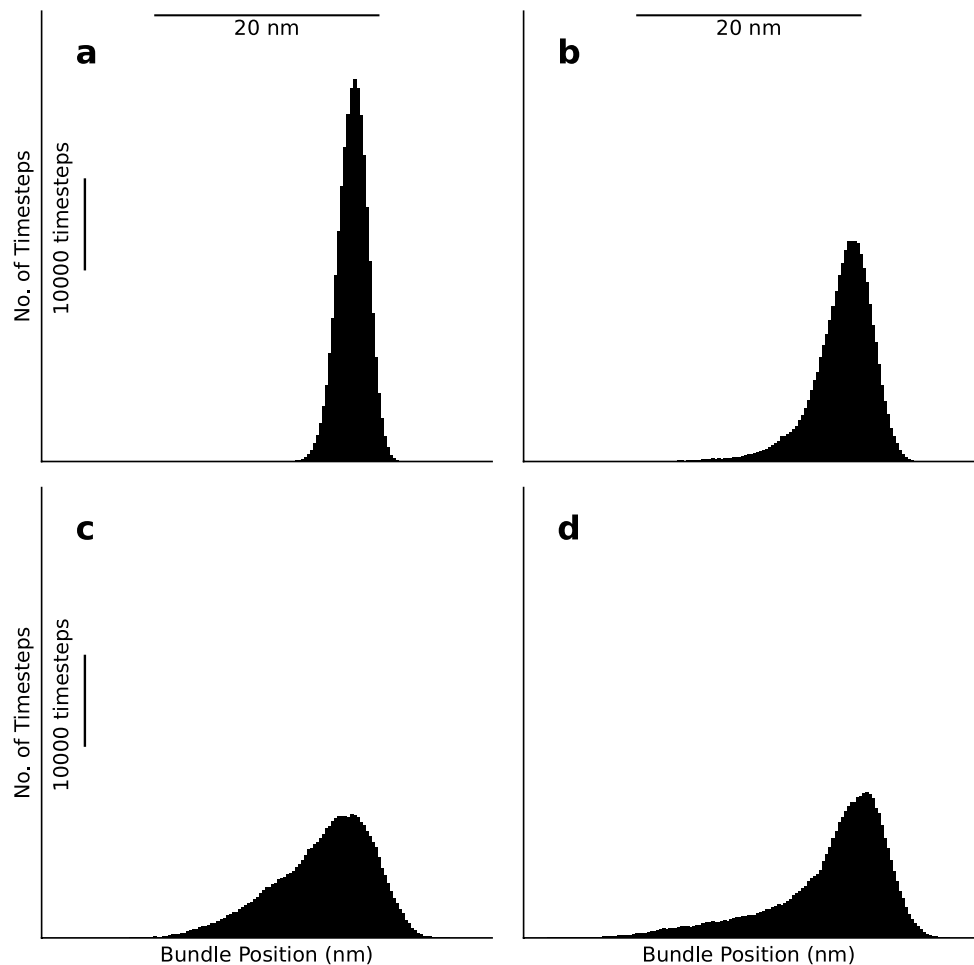
Results

When autonomous oscillators with significant frequency dispersion are strongly coupled, the oscillations may become suppressed through a phenomenon known as amplitude death. It has previously been proposed that this mechanism is responsible for quenching the spontaneous hair-bundle oscillations in the sacculus, an organ which possesses both strong coupling and significant frequency dispersion [23]. Experimental studies have further shown that the presence of a healthy otolithic membrane suppresses innate oscillations exhibited by uncoupled hair bundles. Our model exhibits amplitude death when $K_v = K_d = K$ for all oscillators, describing a properly

functioning sacculus. However, as the coupling coefficient decreases, the suppression weakens, and bundles begin to exhibit spontaneous activity with amplitudes significantly greater than those induced by the thermal noise alone (Fig. 3d, h). These spikes in amplitude increase in both magnitude and frequency with reduction of coupling, which models increasing levels of damage to the tissue (Fig. 3a–h).

We present these statistics in histograms, which display long tails in the negative direction (Fig. 4b–d), becoming more skewed with increasing level of damage relative to the control when there is no membrane damage (Fig. 4a). These drastic spikes in bundle positions from equilibrium have been shown to translate into a change in the opening probability of the transduction channels, which in turn leads to depolarization of the hair cell soma that triggers afferent neural activity (Fig. 5) [4–6]. This increase in the MET channel opening probability with increasing levels of damage can be seen as a right shift of the peaks of the histograms shown in Fig. 6a–d. These results suggest that lowered coupling strength due to otolithic membrane damage, degradation, or absence may lead to the vestibular dysfunction described by Meniere’s disease.

Fig. 4 a–d Histograms of position of a bundle under damaged conditions for $K_d = K, K/5, K/10,$ and $K/15,$ respectively. The traces used to generate these histograms are plotted in black in Fig. 3. Each histogram was produced using a trace from a simulation of 500,000 timesteps representing 10 s



Discussion

Our numerical simulations show that as the coupling strength imposed by the otolithic membrane decreases, hair bundles exhibit abrupt spikes and even intermittent oscillations in their position. This spontaneous activity translates to large fluctuations in the open probability of the transduction channels. Prior work has shown that channel opening leads to depolarization of the hair cell soma and could result in spurious signal detection by the afferent neurons. These results agree with the surgical observation that vestibular drop attacks are correlated with significant damage and degradation of the otolithic membrane in patients with Meniere's disease. Additionally, our findings explain why the absence of a functioning gene for otogelin, an inner-ear structural protein that attaches the otolithic membrane to the underlying tissue, can lead to MD [24, 25]. When functional otogelin proteins are not available, the otolithic membrane is not securely attached to the neuroepithelia and, in some cases, completely detaches. Hence, the extant literature indicates that reduction or

elimination of innate coupling between hair cells underlies a number of symptoms associated with MD.

It has previously been proposed that the vestibular dysfunction associated with Meniere's disease may result from the altered fluid dynamics imposed by endolymphatic hydrops [1, 3]. While both effects may be present in patients suffering from MD, in this study, we focus on a theoretical description of how these symptoms can arise purely from the degradation of the otolithic membrane tissue without the need for forces caused by endolymphatic hydrops. We use a simple numerical model that has previously been developed to describe the active, nonlinear dynamics of hair cells. Although this model was originally proposed to describe the spontaneous oscillations of saccular hair-cell bundles in the bullfrog, the finding that reduced coupling can lead to spontaneous spikes in hair bundle position is very general. Any inter-connected active system in which coupling between the nonlinear elements leads to quiescence can exhibit sudden motion when localized damage removes the quenching of active motility. This has been well studied mathematically but has not been widely applied to the study of Meniere's

Fig. 5 a–d MET channel open probability under damaged conditions for $K_d = K, K/5, K/10,$ and $K/15,$ respectively. The traces used to generate these plots are plotted in black in Fig. 3. Open probabilities are calculated using Eq. 4

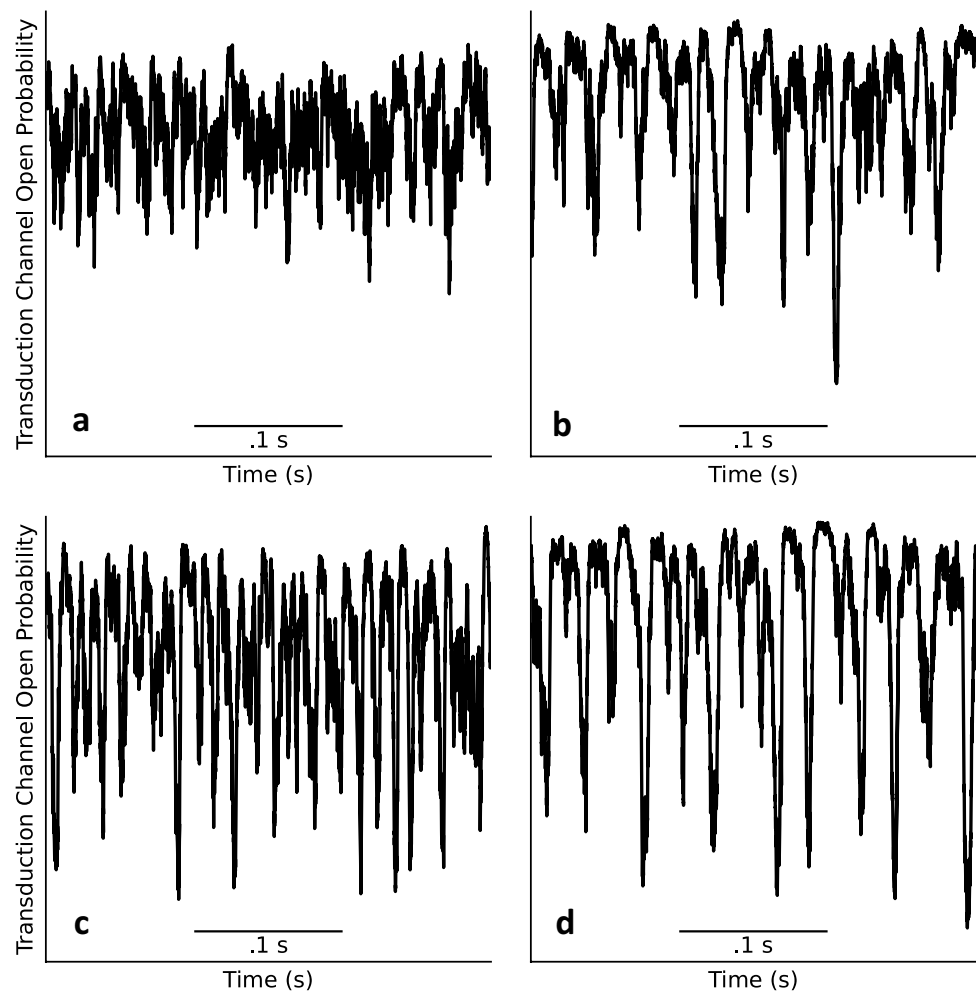
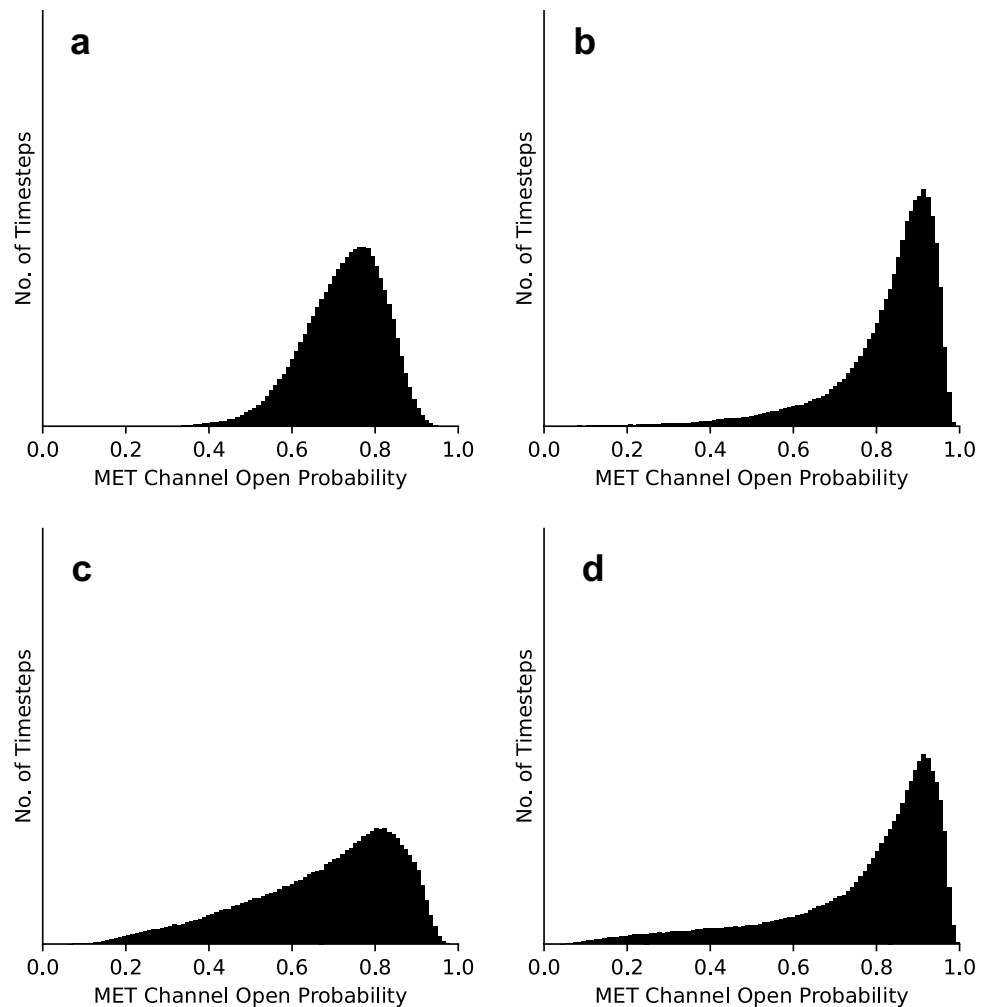


Fig. 6 a–d Histograms of MET channel open probability under damaged conditions for $K_d = K, K/5, K/10$ and $K/15$, respectively. The traces used to generate these plots are plotted in Fig. 5



disease. Furthermore, while the specific mechanisms are different across species, the fundamental dynamics of hair cells used in this model are the transduction mechanism combined with an adaptation process. This can be readily generalized to apply across species. We propose therefore that the results of this model are general and applicable to the mammalian vestibular system. We hence show a possible mechanism by which degradation of coupling can lead to spurious vestibular signals.

Future work entails using animal models to test for this mechanism of spurious detection in groups of active hair cells. The hair-cell bundles can be coupled with artificial membranes of different size, thickness, and properties of the material, to explore the dynamics of various coupled active systems. Alternatively, semi-intact preparations can be used, in which the otolithic membrane is left attached to the hair bundle tips, and one can impose various degrees of damage to the tissue through mechanical stress or chemical digestion of the membrane, thus mimicking the MD symptoms in vitro.

Future computational work entails exploring the effects of various shapes, sizes, and levels of heterogeneity of the damaged region to determine if this model can encompass the full range of observed phenomena associated with the MD.

Conclusions

The results of our numerical simulations suggest that damage to the otolithic membrane of the utricle and/or saccule may be sufficient to induce vestibular drop attacks and the vestibular dysfunction seen in patients with Meniere's disease. These observations agree with prior work showing that patients with damaged/dysfunctional otolithic membranes in the utricle and/or saccule often develop MD, and some experience VDAs. Future experimental work is needed to confirm these results in vitro, and future computational work is needed to determine if the effects of reduced coupling can explain other aspects of Meniere's disease.

Data Availability The relevant code is available on GitHub per reference 25.

Open Access This article is licensed under a Creative Commons Attribution 4.0 International License, which permits use, sharing, adaptation, distribution and reproduction in any medium or format, as long as you give appropriate credit to the original author(s) and the source, provide a link to the Creative Commons licence, and indicate if changes were made. The images or other third party material in this article are included in the article's Creative Commons licence, unless indicated otherwise in a credit line to the material. If material is not included in the article's Creative Commons licence and your intended use is not permitted by statutory regulation or exceeds the permitted use, you will need to obtain permission directly from the copyright holder. To view a copy of this licence, visit <http://creativecommons.org/licenses/by/4.0/>.

References

- Sajjadi H, Paparella MM (2008) Meniere's disease. *The Lancet* 372:406–414
- Calzada AP, Lopez IA, Ishiyama G, Ishiyama A (2012) Otolithic membrane damage in patients with endolymphatic hydrops and drop attacks. *Otol Neurotol* 33:1593–1598
- Ishiyama G, Lopez IA, Sepahdari AR, Ishiyama A (2015) Meniere's disease: histopathology, cytochemistry, and imaging. *Ann N Y Acad Sci* 1343:49–57
- LeMasurier M, Gillespie PG (2005) Hair-cell mechanotransduction and cochlear amplification. *Neuron* 48:403–415
- inner-ear hair-cell mechanotransduction (2019) Ó Maoiléidigh, D. & Ricci, A. J. A Bundle of mechanisms. *Trends Neurosci* 42:221–236
- Vollrath MA, Kwan KY, Corey DP (2007) The micromachinery of mechanotransduction in hair cells. *Annu Rev Neurosci* 30:339–365
- Martin P, Hudspeth AJ (2001) Compressive nonlinearity in the hair bundle's active response to mechanical stimulation. *Proc Natl Acad Sci USA* 98:14386–14391
- Martin P, Hudspeth AJ (1999) Active hair-bundle movements can amplify a hair cell's response to oscillatory mechanical stimuli. *Proc Natl Acad Sci USA* 96:14306–14311
- Benser ME, Marquis RE, Hudspeth AJ (1996) Rapid, active hair bundle movements in hair cells from the bullfrog's sacculus. *J Neurosci* 16:5629–5643
- Martin P, Bozovic D, Choe Y, Hudspeth AJ (2003) Spontaneous oscillation by hair bundles of the bullfrog's sacculus. *J Neurosci* 23:4533–4548
- Martin P, Hudspeth AJ, Jülicher F (2001) Comparison of a hair bundle's spontaneous oscillations with its response to mechanical stimulation reveals the underlying active process. *Proc Natl Acad Sci USA* 98:14380–14385
- Fredrickson-Hemsing L, Strimbu CE, Roongthumskul Y, Bozovic D (2012) Dynamics of freely oscillating and coupled hair cell bundles under mechanical deflection. *Biophys J* 102:1785–1792
- Benser ME, Issa NP, Hudspeth AJ (1993) Hair-bundle stiffness dominates the elastic reactance to otolithic-membrane shear. *Hear Res* 68(2):243–252
- Kondrachuk A, v. (2000) Computer simulation of the mechanical stimulation of the saccular membrane of bullfrog. *Hear Res* 143(1–2):130–138
- Meenderink SWF, Quinones PM, Bozovic D (2015) Voltage-mediated control of spontaneous bundle oscillations in saccular hair cells. *J Neurosci* 35(43):14457–14466
- Dierkes K, Jülicher F, Lindner B (2012) A mean-field approach to elastically coupled hair bundles. *Eur Phys J E* 35(5):37
- Nadrowski B, Martin P, Jülicher F (2004) Active hair-bundle motility harnesses noise to operate near an optimum of mechanosensitivity. *Proc Natl Acad Sci USA* 101:12195–12200
- Ji S, Bozovic D, Bruinsma R (2018) Amphibian sacculus and the forced Kuramoto model with intrinsic noise and frequency dispersion. *Phys Rev E* 97(4):042411
- Yamoah EN, Gillespie PG (1996) Phosphate analogs block adaptation in hair cells by inhibiting adaptation-motor force production. *Neuron* 17:523–533
- Roongthumskul Y, Fredrickson-Hemsing L, Kao A, Bozovic D (2011) Multiple-timescale dynamics underlying spontaneous oscillations of saccular hair bundles. *Biophys J* 101:603–610
- Ramunno-Johnson D, Strimbu CE, Fredrickson L, Arisaka K, Bozovic D (2009) Distribution of frequencies of spontaneous oscillations in hair cells of the bullfrog sacculus. *Biophys J* 96:1159–1168
- <https://github.com/NicholasSenofsky/MD-VDA-Numerical-Model>
- Kim KJ, Ahn KH (2014) Amplitude death of coupled hair bundles with stochastic channel noise. *Phys Rev E Stat Nonlin Soft Matter Phys* 89(4):042703
- Roman-Naranjo P et al (2020) Burden of rare variants in the OTOG Gene in familial Meniere's disease. *Ear Hear* 41(6):1598–1605
- Simmmer MC et al (2000) Targeted disruption of Otog results in deafness and severe imbalance. *Nat Genet* 24:139–143

Publisher's Note Springer Nature remains neutral with regard to jurisdictional claims in published maps and institutional affiliations.